Hindawi Publishing Corporation
International Journal of Photoenergy
Volume 2007, Article ID 87467, 6 pages
doi:10.1155/2007/87467

Research Article

Enhanced Photoelectrochemical Response of Zn-Dotted Hematite

Saroj Kumari,[1] Aadesh P. Singh,[1] Chanakya Tripathi,[2] Diwakar Chauhan,[2] Sahab Dass,[2] Rohit Shrivastav,[2] Vinay Gupta,[3] K. Sreenivas,[3] and Vibha R. Satsangi[1]

[1] *Department of Physics and Computer Science, Faculty of Science, Dayalbagh Educational Institute, Dayalbagh, Agra 282005, India*
[2] *Department of Chemistry, Faculty of Science, Dayalbagh Educational Institute, Dayalbagh, Agra 282005, India*
[3] *Department of Physics and Astrophysics, University of Delhi, Delhi 110007, India*

Received 8 September 2006; Revised 11 January 2007; Accepted 18 March 2007

Recommended by Ignazio Renato Bellobono

Photoelectrochemical response of thin films of α-Fe_2O_3, Zn doped α-Fe_2O_3, and Zn dots deposited on doped α-Fe_2O_3 prepared by spray pyrolysis has been studied. Samples of Zn dots were prepared using thermal evaporation method by evaporating Zn through a mesh having pore diameter of 0.7 mm. The presence of Zn-dotted islands on doped α-Fe_2O_3 surface exhibited significantly large photocurrent density as compared to other samples. An optimum thickness of Zn dots ~230 Å is found to give enhanced photoresponse. The observed results are analyzed with the help of estimated values of resistivity, band gap, flatband potential, and donor density.

1. INTRODUCTION

It is universally accepted that hydrogen is the ideal energy carrier of the future. Photoelectrochemical splitting of water into hydrogen and oxygen on the surface of a photoactive electrode using solar radiation is a potentially clean, and a renewable source for hydrogen fuel. After the pilot experiment of Fujishima and Honda in 1972 on photoassisted water electrolysis using TiO_2 as the photoanode in the photoelectrochemical cell (PEC) for water splitting, many semiconducting materials such as $SrTiO_3$ [1] and WO_3 [2] have been studied for hydrogen production. These electrodes are reported to be stable in aqueous solution, but operate in the UV light and account for only 4% of the incoming solar radiation, and renders the overall process impractically. Unfortunately, small bandgap semiconductors such as Si [3] and CdS [4] decompose under anodic polarization or illumination. Efficient semiconductor materials for this purpose must possess certain characteristics, such as, suitable bandgap energy, flatband potential, over potential losses, stability towards photocorrosion, and suitable physical characteristics.

Iron oxide (α-Fe_2O_3) has a bandgap of ~2.2 eV, which lies in the visible region of solar spectrum and allows utilization of 40% of the incident solar radiation. α-Fe_2O_3 is naturally abundant in the earth's crust, substantially less expensive and has excellent resistance to chemical and photochemical corrosion in aqueous solution [5]. Attempts have been made towards PEC splitting of water using α-Fe_2O_3 prepared by many methods such as pressing powder of Fe_2O_3 [6–8], sputtering [9], and by spray pyrolysis [10–12], but the results obtained from these are not very encouraging in terms of current-voltage characteristics due to two reasons: (a) position of conduction band with respect to redox level of water leading to nonfacilitation of transfer of charge carriers across the junction [13], and (b) short life time of photogenerated minority carriers of α-Fe_2O_3 causing recombination of photogenerated electrons and holes. The properties of iron oxide can be altered by varying the defect chemistry and associated electronic structure through the introduction of extrinsic defects and/or the alteration of the concentration of intrinsic defects by doping [6, 8, 14, 15]. Nanostructured hematite [16] and nanorods [17] have been studied for PEC splitting of water keeping in view that in such systems, the distance, the hole has to diffuse before reaching the interface is only a few nanometers, and the minority carriers can be rapidly captured by the electrolyte present in the nanopores. But lower efficiency was reported in these cases due to poor transport of carriers over the grain boundaries.

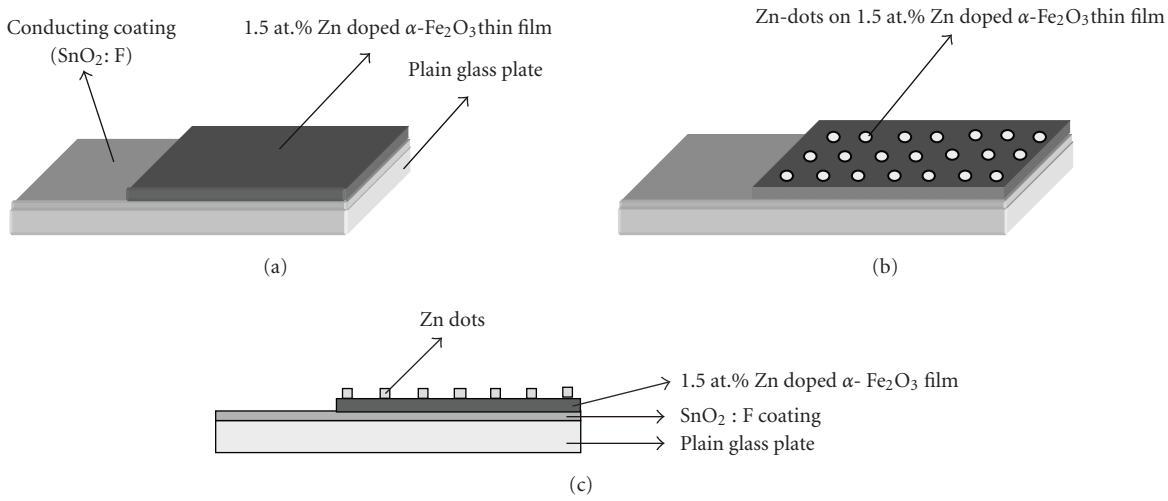

Figure 1: Schematic diagram of Zn-dotted islands on 1.5 at.% Zn-doped α-Fe_2O_3 thin film.

In the present work, modifications of the hematite electrode by doping with zinc, and fabricating Zn-dotted islands of varying heights on the surface of α-Fe_2O_3 thin film electrode have been studied. The thin film structures were used as the working electrodes in the PEC cell, and the presence of zinc in the form of dotted islands on the surface is found to play an important role in the fabricated structure and offers better photocurrent density.

2. EXPERIMENTAL

Zn-doped iron oxide (α-Fe_2O_3) films were deposited by spray pyrolysis [18]. Spray solution was prepared by dissolving 0.15 M iron (III) nitrate [$Fe(NO_3)_3 \cdot 9H_2O$] along with 1.5 at.% $Zn(NO_3)_2 \cdot 6H_2O$ as dopant in double distilled water. This precursor was sprayed with air ($\sim$10 kg cm^{-2}) onto conducting glass substrate (SnO_2 : F) kept at temperature 350°C to get thin film of Zn-doped iron oxide. One-third length of the conducting glass substrate was covered by aluminum foil during spray deposition so that this portion may be used for obtaining electrical contact (Figure 1(a)). Precursor for undoped iron oxide film was prepared without dissolving zinc nitrate. The doped/undoped thin films of Fe_2O_3 were annealed at 500°C for two hours in air. Metallic Zn (in the form of dots) was deposited on the surface of the films using vacuum coating unit. Zn wire (Aldrich, 99.9%) was thermally evaporated and deposited through a mesh having a pore diameter of $\sim$0.7 mm (Figure 1(b)), on the surface of the 1.5 at.% Zn-doped α-Fe_2O_3 films prepared earlier. Top view and transverse view of Zn-dotted films are depicted in Figures 1(b) and 1(c), respectively. The height of Zn dots (islands) was varied in the range of 100 to 260 Å by varying the processing time of thermal evaporation. The heights were controlled and measured by a Quartz crystal film thickness measurement unit (HINDHIVAC, India, Model-DTM-101) during deposition. The surface fraction of the sample covered by Zn dots was 9.62×10^{-2}. The sample details are listed in Table 1. All prepared samples with and without Zn dots were finally annealed at 350°C for 2 hours in air. A continuous layer of Zn was also deposited by the same method on the surface of 1.5 at.% Zn-doped α-Fe_2O_3 without using mesh for comparison.

The electrical contacts on all the samples for PEC measurements were made through a fine copper wire loop attached to the uncovered conducting glass substrate with conducting silver paint. The uncoated area of the conducting glass substrate including the copper wire loop were covered and sealed by an epoxy resin, which was nonconducting and opaque. The entire structure was heated in an oven at 70–80°C to ensure complete drying.

3. RESULTS AND DISCUSSION

The thickness of all the Zn-doped α-Fe_2O_3 thin films was $\sim$1.2 μm as measured by Dektak surface profile measuring system (Veeco Instrument Inc., USA).

The structural characterization of films was carried out using X-ray powder diffractometer (X'PERT Model, Philips, with graphite monochromator) with Cu$-$Kα radiation. The typical XRD pattern of a thin film structure consisting of Zn dots on the Zn-doped hematite film having 230 Å thick Zn dots is shown in Figure 2. Diffraction peaks in the XRD confirmed the formation of single phase of hematite. Additionally some peaks corresponding to underlying SnO_2 : F conducting glass layer are also observed. The major peaks at 2θ angle 33.22° and 35.76° have been identified as peaks corresponding to α-Fe_2O_3, but quite likely these peaks also incorporate within them the peaks corresponding to ZnO, which is the possible conversion of Zn dots to ZnO during thermal treatment. The average crystallite size of hematite as estimated with the help of the Debye-Scherrer equation was found to be $\sim$54 nm for all the samples.

The surface morphology of the prepared samples with and without Zn islands were investigated using atomic force microscope (AFM) of Veeco-D1CP II, USA, and are shown in Figure 3. A smooth and uniform surface morphology

Table 1

Sample identity	Description of samples	Resistivity (Ωcm)	Photocurrent density at 0.7 V/SCE (mA cm^{-2})	V_{on} (mV)	Flatband potential, V_{FB} (mV)	Donor density, N_D(cm^{-3})	Depletion layer width, ω (Å)
A	Undoped α-Fe_2O_3	4.0×10^6	0.061	660.5	−580	21.4×10^{19}	11.0
B	1.5 at.% Zn-doped α-Fe_2O_3	2.6×10^7	0.321	420.5	−710	12.0×10^{19}	26.2
C	100 Å thick Zn dots on sample B	1.5×10^7	0.32	260.5	−630	12.0×10^{19}	22.5
D	200 Å thick Zn dots on sample B	5.9×10^6	0.701	294.5	−650	14.0×10^{19}	21.3
E	230 Å thick Zn dots on sample B	5.7×10^6	1.282	306.5	−680	15.0×10^{19}	18.6
F	260 Å thick Zn dots on sample B	9.2×10^6	0.576	272.5	−680	15.0×10^{19}	22.5
G	α-Fe_2O_3/ZnO	—	0.462	495.5	—	—	—

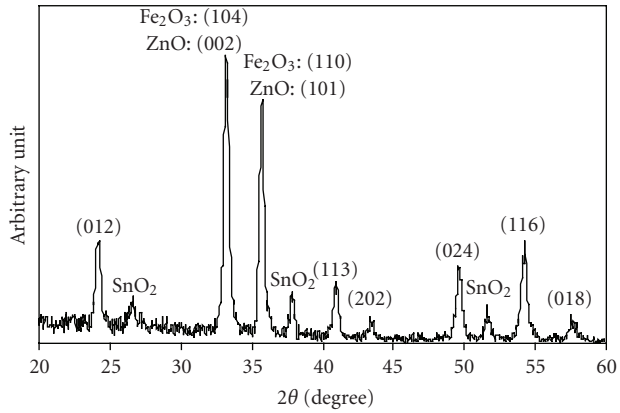

Figure 2: X-ray diffraction pattern for Zn-dotted α-Fe_2O_3 (sample E).

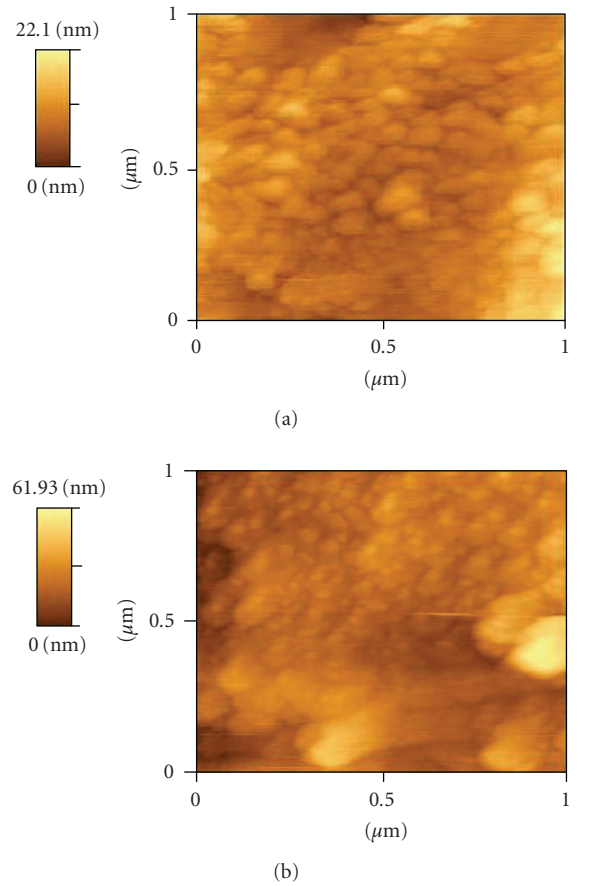

Figure 3: AFM images for the Zn dot deposited on 1.5 at.% Zn-depod hematite, (sample E): (a) hematite film without dots and (b) area of Zn dot.

having spherical grains are evident from the AFM images. The estimated value of the average grain sizes are found to be about 62–67 nm, which closely matches with the average particle/grain size calculated by Scherrer equation using XRD data. The surface roughness observed in the Zn-doped hematite samples was found to be low (< 10 nm). The morphology of Zn islands was observed rough with extensive granular structures (Figure 3(b)).

The bandgap energy was calculated from the absorbance data of thin films recorded by a UV-VIS spectrophotometer (Shimadzu, UV-1601) using the following equation [19–21]:

$$(\alpha h\upsilon) = A(h\upsilon - E_g)^n. \quad (1)$$

Here, α is the absorption coefficient near the absorption edge, A is a constant, υ is the frequency, E_g is the bandgap of the material and n is a constant related to the type of optical transition, $n = 2$ for indirect transition and $n = 1/2$ for direct transition. Hematite has been suggested to have an indirect bandgap [19, 22]. However, a direct bandgap for hematite is also reported [23]. The absorbance spectra of all the prepared samples were recorded as a function of wavelength, and the bandgap energy was estimated from the intercept of the linear portion of the plot between $(\alpha h\upsilon)^{1/2}$ versus $h\upsilon$. The typical absorbance spectra and the plot of $(\alpha h\upsilon)^{1/2}$ versus $h\upsilon$ for sample E are shown in Figures 4 and 5, respectively. The absorbance spectra showed a prominent absorption at around 546 nm in all the prepared samples. The estimated values of the bandgap of all the samples (A to F) were found to be about 1.97 eV, which closely match with the earlier reported values for hematite films [19, 23].

Resistivity of any material depends on the mobility of charge carriers and charge concentration. Resistivity of all the samples was calculated from the current-voltage characteristics in PEC cell using a potentiostat. Total ohmic resistance

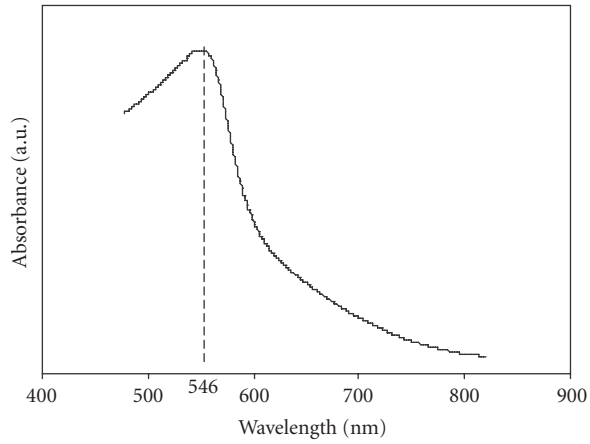

Figure 4: Absorbance curve for Zn-dotted α-Fe_2O_3 (sample E).

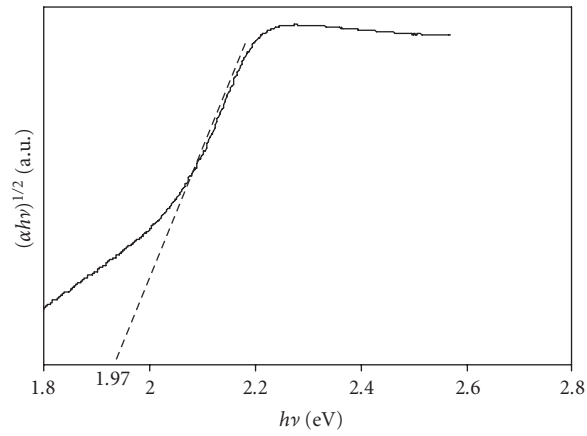

Figure 5: $(\alpha h\nu)^{1/2}$ versus $h\nu$ curve for Zn-dotted α-Fe_2O_3 (sample E).

offered to the flow of current in the circuit is due to the thin film sample, the electrolyte in which film is dipped and platinum counter electrode. Resistances due to the platinum counter electrode and electrolyte have been neglected as both have large amount of charge carriers. The contribution to the measured total resistance was mainly due to the fabricated thin film structure on doped α-Fe_2O_3 films with/without Zn-dotted islands on the surface. Specific resistivity calculated from the current-voltage characteristics for all the samples are compiled in Table 1. The resistivity is found to increase by one order with Zn doping and is attributed to the substitution of Zn^{2+} ion in place of Fe^{3+} ions thereby resulting in loss of an electron. The presence of Zn-dotted islands on the film surface shows a decrease in resistivity due to difference in the work function of two layers. However, a slight increase in resistivity is observed after loading with 260 Å thick Zn-dotted islands. The long evaporation time for 260 Å thick-dotted islands may lead to the interdiffusion of Zn inside the iron oxide near the interface resulting in loss of charge carrier. It is important to note that all samples exhibited n-type electrical conductivity.

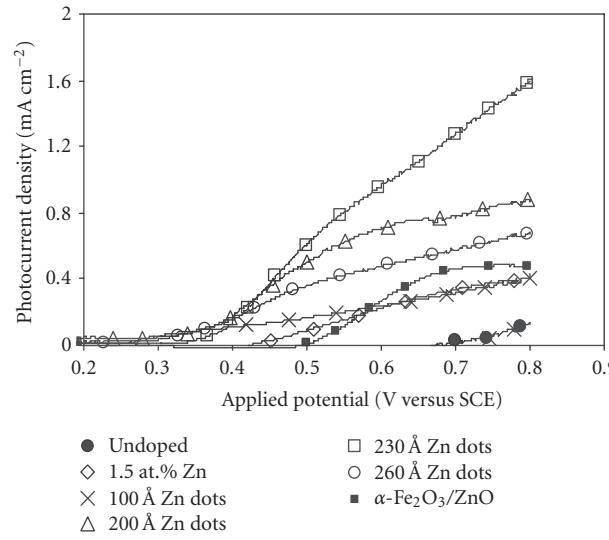

Figure 6: Photocurrent density versus applied potential curve for α-Fe_2O_3 (all samples) in 13 pH NaOH electrolyte solution.

3.1. Photoelectrochemical studies

Photoelectrochemical response from the samples has been studied in NaOH (pH 13). The PEC cell consisted of a semiconductor electrode, the electrolyte, the platinum counter electrode, and a reference electrode (saturated calomel electrode—Model K0077, USA.). The prepared thin film structures were illuminated with 150 W tungsten lamp (white light source) and current-voltage curves were recorded using a potentiostat (PAR, USA; Model-VERSASTAT II).

The photoresponse of hematite depends on the number of photogenerated charge carriers, lifetime of photogenerated charge carriers, and the catalytic behavior at the interface of the doped iron oxide and electrolyte. Observed photoelectrochemical (PEC) response of all the samples is shown in Figure 6. The Zn-doped hematite film exhibited enhanced photoresponse, which was further improved with the presence of Zn-dotted islands on its surface. The values of photocurrent density obtained at a bias of 0.7 V/SCE are listed in Table 1 for all the samples. A continuous increase in photocurrent density is observed as the height of the Zn dots is increased from 100 to 230 Å. Thin film structures with ∼230 Å thick Zn dots exhibited an enhanced photoresponse by one order of magnitude in comparison to both the undoped, and the 1.5 at.% Zn-doped iron oxide thin films (Table 1). This photocurrent density is quite large as compared to the values reported earlier [6, 8].

The enhancement in photoresponse is probably due to the catalytic activity of ZnO-dotted islands form on the surface of hematite. The catalytic activity was found to increase with the increase in thickness of Zn-dotted islands up to 230 Å. However, the observed decrease in the photoresponse of film having 260 Å thick-dotted islands could be correlated to the interdiffusion of Zn inside the hematite near the interface. The interdiffusion of Zn is expected during the long processing time of thermal evaporation for thick

islands. The area of uncovered hematite surface in the prepared sample was reduced due to interdiffusion of Zn and resulted in a decreased photoresponse. It indicates that an optimum height of dotted islands is required on the surface of the hematite film to obtain an enhanced photoelectrochemical response. The enhanced photoresponse of Zn-dotted islands on hematite may be attributed to the activation of the photoelectrochemical activity on the uncovered hematite layer due to the presence of catalytic dotted islands.

To further analyze the role of catalytic Zn on iron oxide thin films a 230 Å thick continuous layer of Zn was deposited on the surface of doped hematite under similar processing conditions. The presence of a continuous film of Zn on hematite layer increases the photoresponse in comparison to uncovered Zn-doped hematite layer, whereas it is lower with respect to dotted Zn.

It is observed that V_{on}, the onset voltage where photocurrent starts, is lower in Zn-doped samples, and is further lowered with the presence of Zn-dotted islands on the surface as compared to undoped samples (Table 1). This shows that the Zn dots on the surface of doped α-Fe_2O_3 film are not only enhancing the catalytic activity, but also playing an important role in shifting the band edges under illumination towards the favorable side.

Capacitance (C) at the semiconductor/electrolyte junction was measured using an LCR meter (Agilent Technology—Model 4263B) at varying electrode potentials for AC signal frequency of 1 kHz, and the Mott-Schottky plot ($1/C^2$ vs applied potential) were obtained and analyzed for all the samples. The flatband potential (V_{FB}) and donor density (N_D) were calculated using Mott-Schottky plot ($1/C^2$ versus applied potential) at the semiconductor/electrolyte interface using the equation [24–26],

$$\frac{1}{C^2} = \left(\frac{2}{q\varepsilon_o\varepsilon N_D}\right)\left(V_{app} - V_{FB} - \frac{kT}{q}\right), \tag{2}$$

where ε_o is the permittivity of free space, V_{app} is the applied potential, ε is the dielectric constant of the semiconductor, and kT/q is the temperature dependent term. Slope of the Mott-Schottky plots yielded the values of donor density, and the intercept of the tangent drawn on the curve in the negative bias region on the potential axis is utilized to calculate the flatband potential. Depletion width was calculated using the values of junction capacitance at the semiconductor/electrolyte interface at zero bias voltage using the formula

$$\omega = \frac{\varepsilon\varepsilon_o}{C}, \tag{3}$$

where C is the junction capacitance. Figure 7 depicts the Mott-Schottky plot for samples A, B, and E at 1 kHz frequency. The estimated values of flatband potential (V_{FB}), donor density (N_D), and depletion layer width (ω) for all samples (A, B, C, D, E, F, and G) have been summarized in Table 1.

In comparison to the undoped hematite thin film (sample A), the Zn-doped film (sample B) exhibited a decrease in donor density, and an increase in both the flatband potential and depletion layer width. Furthermore, the presence of

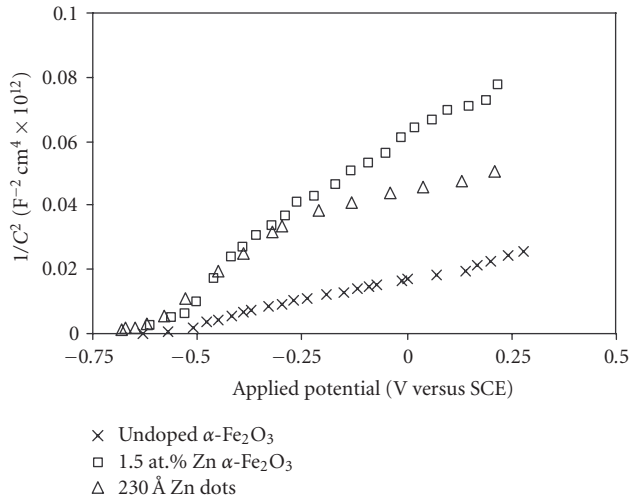

Figure 7: Mott-schottky plot under darkness in 13 pH NaOH at frequency 1 kHz.

Zn-dotted islands on the surface of the Zn doped hematite film (samples C to F) resulted in an insignificant change in the junction properties, except a significant reduction in the V_{on} potential (Table 1). The reduction in the potential (V_{on}) due to Zn doping and Zn dots on the surface of the hematite electrode clearly indicates its catalytic nature that led to a significant enhancement in the photocurrent density (Figure 6). A plausible explanation for enhanced photoelectrochemical response could be related to the fact that Zn-dotted islands when annealed get converted to a wide bandgap ZnO, and acts as an efficient catalyst for the swift migration of the photogenerated charge carriers. An increase in the catalytic activity is observed with increasing height of zinc dotted islands and results in a continuous enhancement in the photoresponse behavior. However, the observed decrease in the photoresponse of the film having 260 Å (sample F) thick dotted islands could be correlated to the interdiffusion of Zn inside the hematite near the interface. The area of uncovered hematite surface in the prepared sample was reduced due to interdiffusion of Zn and results in a decrease the photoresponse.

4. CONCLUSIONS

The present study clearly highlights the advantage of loading Zn-dotted islands on the surface of α-Fe_2O_3 electrodes in comparison to Zn-doped α-Fe_2O_3 in terms of offering enhanced photoresponse for the PEC cell applications. The ZnO was found to act as the catalyst for enhancing the photoresponse of the hematite layer. The presence of Zn-dotted islands on the doped α-Fe_2O_3 film surface apparently shifts the band edges towards the favorable side under illumination and this may be a reason behind its role as catalyst for efficient charge transfer reactions for the hydrogen and oxygen evolution at semiconductor/electrolyte interface. Further work is in progress to understand the influence of dotted islands of other catalyst materials and the mechanism involved.

ACKNOWLEDGMENTS

The financial assistance from Department of Science and Technology (DST), India, is gratefully acknowledged, and the authors are grateful to Dr. R. K. Sharma, Solid State Physics Laboratory (SSPL), Delhi, for the XRD measurements on the samples.

REFERENCES

[1] P. Salvador, C. Gutiérrez, G. Campet, and P. Hagenmuller, "Influence of mechanical polishing on the photoelectrochemical properties of $SrTiO_3$ polycrystalline anodes," *Journal of the Electrochemical Society*, vol. 131, no. 3, pp. 550–555, 1984.

[2] C. Santato, M. Ulmann, and J. Àugustynski, "Photoelectrochemical properties of nanostructured tungsten trioxide films," *The Journal of Physical Chemistry B*, vol. 105, no. 5, pp. 936–940, 2001.

[3] C. Lévy-Clément, A. Lagoubi, M. Neumann-Spallart, M. Rodot, and R. Tenne, "Efficiency and stability enhancement of n-Si photoelectrodes in aqueous solution," *Journal of the Electrochemical Society*, vol. 138, no. 12, pp. L69–L71, 1991.

[4] H. S. Mansur, F. Grieser, M. S. Marychurch, S. Biggs, R. S. Urquhart, and D. N. Furlong, "Photoelectrochemical properties of 'Q-state' CdS particles in arachidic acid Langmuir-Blodgett films," *Journal of the Chemical Society, Faraday Transactions*, vol. 91, pp. 665–672, 1995.

[5] D. E. Scaife, "Oxide semiconductors in photoelectrochemical conversion of solar energy," *Solar Energy*, vol. 25, no. 1, pp. 41–54, 1980.

[6] C. Leygraf, M. Hendewerk, and G. A. Somorjai, "Mg- and Si-doped iron oxides for the photocatalyzed production of hydrogen from water by visible light ($2.2\ \text{eV} \leq h\nu \leq 2.7\ \text{eV}$)," *Journal of Catalysis*, vol. 78, no. 2, pp. 341–351, 1982.

[7] K. Gurunathan and P. Maruthamuthu, "Photogeneration of hydrogen using visible light with undoped/doped α-Fe_2O_3 in the presence of methyl viologen," *International Journal of Hydrogen Energy*, vol. 20, no. 4, pp. 287–295, 1995.

[8] V. M. Aroutiounian, V. M. Arakelyan, G. E. Shahnazaryan, G. M. Stepanyan, J. A. Turner, and O. Khaselev, "Investigation of ceramic $Fe_2O_3\langle Ta\rangle$ photoelectrodes for solar energy photoelectrochemical converters," *International Journal of Hydrogen Energy*, vol. 27, no. 1, pp. 33–38, 2002.

[9] S. Virtanen, P. Schmuki, H. Böhni, P. Vuoristo, and T. Mantyla, "Artificial Cr- and Fe-oxide passive layers prepared by sputter deposition," *Journal of the Electrochemical Society*, vol. 142, no. 9, pp. 3067–3072, 1995.

[10] K. Itoh and J. O'M. Bockris, "Stacked thin-film photoelectrode using iron oxide," *Journal of Applied Physics*, vol. 56, no. 3, pp. 874–876, 1984.

[11] S. U. M. Khan and J. Akikusa, "Photoelectrochemical splitting of water at nanocrystalline $n - Fe_2O_3$ thin-film electrodes," *The Journal of Physical Chemistry B*, vol. 103, no. 34, pp. 7184–7189, 1999.

[12] T. Lindgren, L. Vayssieres, H. Wang, and S.-E. Lindquist, "Photo-oxidation of water at hematite electrodes," in *Chemical Physics of Nanostructured Semiconductors*, A. I. Kokorin and D. W. Bahnemann, Eds., pp. 83–110, VSP, Leiden, The Netherlands, 2003.

[13] N. M. Dimitrijević, D. Savić, O. I. Mićić, and A. J. Nozik, "Interfacial electron-transfer equilibria and flatband potentials of $\alpha - Fe_2O_3$ and TiO_2 colloids studied by pulse radiolysis," *Journal of Physical Chemistry*, vol. 88, no. 19, pp. 4278–4283, 1984.

[14] V. M. Aroutiounian, V. M. Arakelyan, A. G. Sarkissyan, G. E. Shahnazaryan, G. M. Stepanyan, and J. A. Turner, "Photoelectrochemical characteristics of Fe_2O_3 photoelectrodes doped with elements of forth group," *Russian Journal of Electrochemistry*, vol. 35, no. 8, pp. 963–968, 1999.

[15] A. G. Sarkissyan, G. E. Shahnazaryan, V. M. Arakelyan, V. M. Aroutiounian, and K. H. Begoyan, "Impedance of the electrochemical cell with a titanium-doped Fe_2O_3 semiconductor electrode," *Russian Journal of Electrochemistry*, vol. 33, no. 7, p. 753, 1997.

[16] U. Björksten, J. Moser, and M. Grätzel, "Photoelectrochemical studies on nanocrystalline hematite films," *Chemistry of Materials*, vol. 6, no. 6, pp. 858–863, 1994.

[17] L. Vayssieres, N. Beermann, S.-E. Lindquist, and A. Hagfeldt, "Controlled aqueous chemical growth of oriented three-dimensional crystalline nanorod arrays: application to iron(III) oxides," *Chemistry of Materials*, vol. 13, no. 2, pp. 233–235, 2001.

[18] Y. S. Chaudhary, S. A. Khan, R. Shrivastav, et al., "Modified structural and photoelectrochemical properties of 170 MeV Au^{13+} irradiated hematite," *Thin Solid Films*, vol. 492, no. 1-2, pp. 332–336, 2005.

[19] J. E. Turner, M. Hendewerk, J. Parmeter, D. Neiman, and G. A. Somorjai, "The characterization of doped iron oxide electrodes for the photodissociation of water," *Journal of the Electrochemical Society*, vol. 131, no. 8, pp. 1777–1783, 1984.

[20] R. H. Misho and W. A. Murad, "Band gap measurements in thin films of hematite Fe_2O_3, pyrite FeS_2 and troilite FeS prepared by chemical spray pyrolysis," *Solar Energy Materials and Solar Cells*, vol. 27, no. 4, pp. 335–345, 1992.

[21] Y. S. Chaudhary, A. Agrawal, R. Shrivastav, V. R. Satsangi, and S. Dass, "A study on the photoelectrochemical properties of copper oxide thin films," *International Journal of Hydrogen Energy*, vol. 29, no. 2, pp. 131–134, 2004.

[22] J. C. Launay and G. Horowitz, "Crystal growth and photoelectrochemical study of Zr-doped α-Fe_2O_3 single crystal," *Journal of Crystal Growth*, vol. 57, no. 1, pp. 118–124, 1982.

[23] N. Beermann, L. Vayssieres, S.-E. Lindquist, and A. Hagfeldt, "Photoelectrochemical studies of oriented nanorod thin films of hematite," *Journal of the Electrochemical Society*, vol. 147, no. 7, pp. 2456–2461, 2000.

[24] S. M. Wilhelm, K. S. Yun, L. W. Ballenger, and N. Hackerman, "Semiconductor properties of iron oxide electrodes," *Journal of The Electrochemical Society*, vol. 126, no. 3, pp. 419–424, 1979.

[25] S. S. Kocha, J. A. Turner, and A. J. Nozik, "Study of the Schottky barrier and determination of the energetic positions of band edges at the n- and p-type gallium indium phosphide electrode — electrolyte interface," *Journal of Electroanalytical Chemistry*, vol. 367, no. 1-2, pp. 27–30, 1994.

[26] J. H. Kennedy and K. W. Frese Jr., "Flatband potentials and donor densities of polycrystalline α-Fe_2O_3 determined from Mott-Schottky plots," *Journal of the Electrochemical Society*, vol. 125, no. 5, pp. 723–726, 1978.